Int J Adv Manuf Technol (2009) 45:935–943
DOI 10.1007/s00170-009-2024-9

ORIGINAL ARTICLE

# Three-dimensional heat transfer analysis of LENS$^{TM}$ process using finite element method

**V. Neela · A. De**

Received: 9 June 2008 / Accepted: 16 March 2009 / Published online: 26 March 2009


**Abstract** Laser-engineered net shaping, referred to as LENS$^{TM}$ process, is an additive manufacturing technique for building metallic parts, layer by layer, by direct deposition of metal powders in a melt pool created by a focused laser beam. The process involves rapid melting and solidification of a controlled amount of injected metal powders as a laser beam scans over each layer building the structure from the bottom to the top. Due to its unique capability to deposit precise amounts of powder material at a desired location, the LENS$^{TM}$ process finds potential application in rapid tooling, prototyping, precision repair work, and manufacture of complex, intricate components with varying compositions. The peak temperature and thermal cycle experienced by each layer influence the final mechanical properties and dimensional accuracy of the part. An understanding and quantitative knowledge of the peak temperature, melt pool dimensions, and thermal cycles experienced in the deposited layers are essential for a priori selection of the process parameters in LENS$^{TM}$ technique. It is important to ensure that the deposited layers have the desired dimensions, good interlayer bonding, and requisite mechanical properties. In an attempt to understand the process parameters to be used in achieving the desired nature of deposition, a three-dimensional model is developed based on finite element method to numerically simulate heat transfer phenomenon in LENS$^{TM}$ process considering deposition of SS316 powders on a substrate of the same material. The computed temperature profiles are first validated with experimental results reported in the literature. The influence of process parameters on peak temperature, thermal cycles, and melt pool dimensions are studied subsequently. The continuous movement of laser and synchronized activation of elements depicting addition of powder particles are incorporated through an externally written user subroutine and using the element deactivation and activation features in the commercial finite element software ABAQUS 6.7. A unique non-dimensional parameter specific to LENS$^{TM}$ process is defined considering the combined influence of process parameters and material properties. The non-dimensional parameter is further used to serve as a guideline for the selection of appropriate process parameters that can result in a steady melt pool dimension, thereby ensuring a target layer width with good interlayer bonding.

**Keywords** LENS$^{TM}$ technique · Direct metal deposition · Heat transfer · Finite element method

V. Neela · A. De (✉)
Mechanical Engineering Department, IIT Bombay,
Bombay, India
e-mail: amit@iitb.ac.in

## 1 Introduction

A typical laser-engineered net shaping (LENS$^{TM}$) setup is made up of a substrate and an assembly unit consisting of a laser beam and powder delivery nozzle(s) encapsulated within an inert gas glove box. In this technique, a three-dimensional computer-aided design model of the component is first converted into a stack of two-dimensional layers representing the path to be followed to build each layer. A relative motion, referred to as scanning velocity hereafter, is imposed between the substrate and the assembly unit. The focused laser beam creates a melt pool into which the metal powder particles are simultaneously injected. As the laser beam moves away, the melt pool solidifies, rapidly forming a continuous single line structure onto the substrate. Once the first layer is built, subsequent layers are deposited on the

same. After the deposition of each layer, the powder delivery nozzle(s) and laser beam assembly unit is incremented vertically upward by a small increment. Thus, a three-dimensional structure is built layer by layer from the bottom to the top [1–3].

Since the LENS$^{TM}$ process involves concentrated localized heating, high peak temperatures, and cooling rate, accurate measurements of thermal cycles are considered to be difficult. Griffith et al. [4] measured temperatures through inserted thermocouples during the fabrication of a H13 tool steel hollow box. High-speed thermal imaging techniques were used to capture the thermal history during fabrication of a SS316 thin wall structure [5, 6]. The measured temperatures and the thermal cycles were correlated with the hardness of the deposited material [4, 5]. Thermal gradients and cooling rates were derived from the temperature profiles, and the influence of laser power on peak temperature and cooling rates were also reported by Hoffmeister et al. [6].

Considering the difficulties associated with the accurate measurement of temperature, researchers have subsequently attempted to numerically simulate the thermal behavior observed in LENS$^{TM}$ process using finite element method [6–13]. Hoffmeister et al. [6] and Ye et al. [9] simulated the thermal behavior in LENS$^{TM}$ process using a three-dimensional conduction heat transfer model. Material addition was assumed to be at melting temperature, and the substrate was held constant at 573 K [6] and 323 K [9] throughout the simulation. The authors did not consider temperature dependence of material properties and the latent heat of melting or solidification. Vasinonta et al. [7] reported a two-dimensional heat transfer model considering the laser beam as a point heat source. Costa et al. [8] developed a thermo-kinetic model coupling the heat transfer analysis with phase transformation kinetics to estimate the microstructure and hardness distribution in a ten-layered SS420 wall structure. The influence of the substrate size and of idle time in between the deposition of two successive layers on the hardness and phase distribution in the part were studied. Wang et al. [10, 11] reported the influence of material properties on the computed temperature profiles of the deposited layers. Grujicic et al. [12] reported that the increase in laser power and in-flight time of powder particles would help in faster melting of the powder particles. Peyre et al. [13] used an analytical relation to estimate the geometry of the deposited layer during the building of a 25-layered structure of Ti alloy.

Majority of the heat transfer models reported in the literature for the thermal analysis of LENS$^{TM}$ process have neglected the energy distribution in the laser beam and instead considered the powder particles at melting temperature as the source of heat [6–10]. The temperature dependence of material properties and the influence of latent heat are rarely considered [6, 9, 10, 12]. Often, the entire substrate, irrespective of its size, is forced to remain at ambient or some lower temperature throughout the deposition process, thereby imposing an unrealistic thermal boundary condition [6, 7, 9–11]. Although the commercial finite element packages were mostly used to develop the heat transfer models, synchronization between activation of new elements, scanning velocity, mesh size, and mass flow rate of powder particles were not outlined explicitly [6–13]. The transient heat transfer model developed in the present work using ABAQUS 6.7 aims at overcoming some of the lacunae of the previously reported models.

## 2 Theoretical formulation

Figure 1 shows a schematic view of the setup used in LENS$^{TM}$ process and the typical boundary conditions that are considered in the present heat transfer analysis. Three-dimensional transient heat conduction equation in Cartesian coordinate system can be given as [14]:

$$\frac{\partial}{\partial x}\left(k\frac{\partial T}{\partial x}\right)+\frac{\partial}{\partial y}\left(k\frac{\partial T}{\partial y}\right)+\frac{\partial}{\partial y}\left(k\frac{\partial T}{\partial z}\right)=\rho C\frac{\partial T}{\partial t} \tag{1}$$

where $\rho$, $C$, $k$, $T$, and $t$ refer, respectively, to density, specific heat, thermal conductivity, temperature, and time variables. The boundary condition can be represented mathematically as [14]:

$$k_n\frac{\partial T}{\partial n}-q+h_{conv}(T-T_a)+\sigma\varepsilon\left(T^4-T_{\mathrm{a}}^4\right)=0 \tag{2}$$

where $n$ refers to the direction normal to surface; $k_n$, $h$, $\varepsilon$, $\sigma$, and $T_{\mathrm{a}}$ refer to thermal conductivity, surface heat transfer coefficient, emissivity, Stefan–Boltzmann constant, and the ambient temperature, respectively. The term $q$ stands for the heat input due to the laser beam that is considered to follow a Gaussian distribution as:

$$q=\frac{P\eta d}{\pi\times r_{\mathrm{lb}}^2}\exp\left(-\frac{dr^2}{r_{\mathrm{lb}}^2}\right) \tag{3}$$

where $r^2=x^2+y^2$; $P$, $\eta$, $r_{\mathrm{lb}}$ and $d$ refer to the laser power, absorption coefficient of the laser beam, effective radius of laser beam, and the beam distribution parameter, respectively. The values of $\eta$, $d$, and $r_{\mathrm{lb}}$ are considered as 0.50, 1.5, and 1.0 mm, respectively. The values of surface heat transfer coefficient ($h_{\mathrm{conv}}$) and emissivity ($\varepsilon$) are taken as 10 W/m$^2$K and 0.35, respectively [10]. The initial temperature of the entire part is assumed to be at $T_0$, which can be expressed as:

$$T(x,y,z,0)=T_0 \tag{4}$$

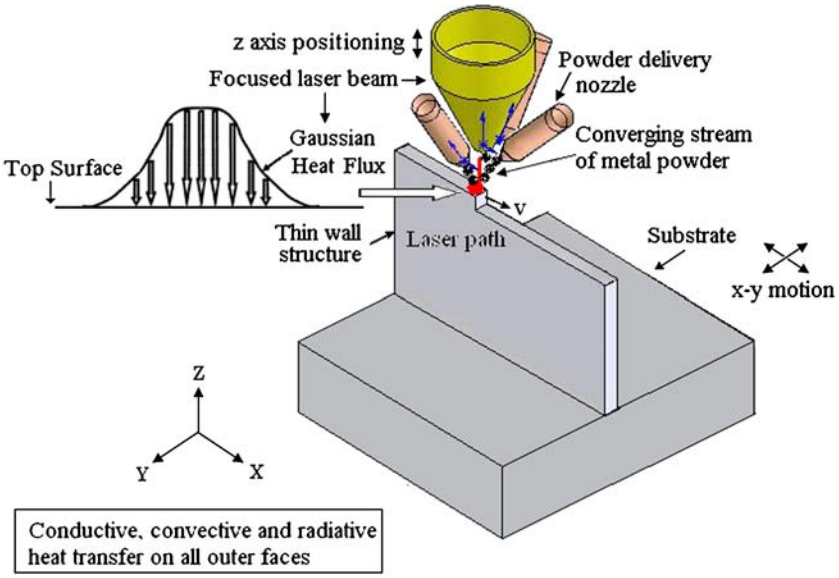


**Fig. 1** Schematic view of the single-line multilayered solution domain and the boundary conditions

where $T_0$=300 K. The governing Eq. 1, along with the boundary condition 2, is discretized to a set of algebraic equations in matrix form to solve for unknown temperature field in the domain considered for solution [14].

A flow chart showing various steps in the computational scheme employed in the present study is given in Fig. 2. The entire deposition process is modeled as a multistep transient heat transfer analysis where each time step is further divided into a number of smaller time increments. The continuous additions of metal powders are considered by means of successive discrete addition of new set of elements into the computational domain at the beginning of each time step, which is fixed such that the laser beam scans a distance equal to a set of newly activated elements. The number of elements to be activated at each time step is determined from the volume of powder materials expected to enter the melt pool during that time step, which depends on powder mass flow rate ($f$), powder use efficiency (considered to be 60%), and scanning velocity ($v$). Three-dimensional eight-node linear brick heat diffusion element (DC3D8) with nodal temperature as the degree of freedom is used for modeling. The laser beam is modeled as a moving surface heat flux with a non-uniform, Gaussian energy distribution. A user subroutine, DFLUX, is used to compute the location of the center of the laser beam and the energy distribution on the incident surface at that time instant. The computed temperature profiles and their sensitivity to various process parameters are studied using the developed model.

## 3 Results and discussions

The temperature distributions are first computed corresponding to the deposition of a multilayered thin wall structure (length/width/height ~12:2:6.25 mm) into a substrate (length/width/height ~12:6:2 mm) using a laser power and scanning velocity of 275 W and 7.62 mm/s, respectively. Hoffmiester et al. [6] measured temperature profiles along the

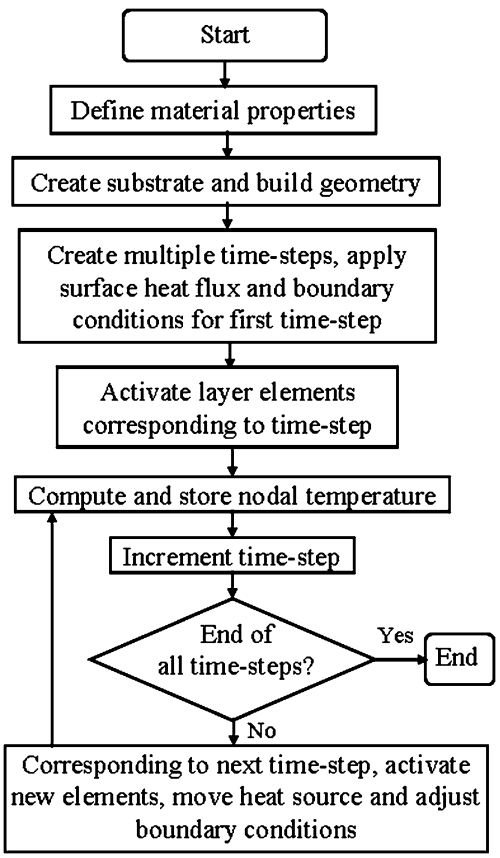


**Fig. 2** Flow chart showing various steps involved in the heat transfer model

top surface of a deposited layer in a similar layer and substrate dimensions, although the corresponding laser beam diameter, absorption coefficient, and powder mass flow rate are not explicitly mentioned. Hence, an average powder mass flow rate of 3 g/min is considered for the present calculation, considering a typical range of 2–6 g/min of the same reported in the contemporary literatures [8, 13]. A layer increment of 250 μm is followed from Hoffmiester et al. [5, 6], and to correlate the same, two layers of eight-node brick elements (DC3D8), each of size 0.125 × 0.125 × 0.125 mm (height), are used to simulate the deposition of each layer. The deposition of the full length (~12 mm) of each layer is completed in six time steps and 512 new elements are activated in each time step ($\Delta t$~0.266 s). An idle time of 5 s between the completion of one layer and the beginning of the subsequent top layer is assumed. A full built height of 6.25 mm is simulated considering deposition of 25 layers and also assuming temperature-dependent material properties of SS316 (Table 1).

Figure 3 depicts the computed results of the temperature profile against the corresponding measured results [6] at a location 1.6 mm away from the center of the laser beam along the topmost layer. The horizontal line in Fig. 3 indicates the liquidus (melting) temperature of SS316 (1,733 K) and meets both the computed and the corresponding measured temperature profiles at their point of intersection. A good agreement between the computed and the corresponding measured melt pool size (~0.75 mm) is thus indicated. Moreover, a fair agreement between the overall computed and the corresponding measured temperature profiles [6] possibly supports the numerical model to be utilized further to study the influence of process parameters on the thermal history during LENS$^{TM}$ process.

Figure 4a shows the computed thermal cycles experienced at different linear locations (3, 6, 9, and 12 mm) on the first layer corresponding to a laser power of 400 W, focused beam radius of 1 mm, scanning velocity of 10 mm/s, and a powder mass flow rate of 4 g/min with 60% catchment efficiency. Figure 4b depicts similar computed thermal cycles on the same locations, however, during the building of the first to eighth layers corresponding to the same set of process variables. It is observed in Fig. 4a that as the laser beam reaches or is near a particular location, peak temperature shoots to nearly 2,100 K followed by a rapid cooling as the beam moves away. Figure 4b indicates that the peak temperature along the first layer reduces continually as the build height increases and the laser beam also moves up. However, the resident temperature of any layer increases continually. The resident temperature refers to the temperature attained by the just deposited layer before the deposition of the next layer starts, and thus, the same is significantly influenced by the idle time used between the depositions of two successive layers. The computed temperature history in Fig. 4b conforms to a duration of 1.2 s for the deposition of each layer and an idle time of 5 s between two successive layers, leading to a total time of 44.6 s for completely depositing eight layers.

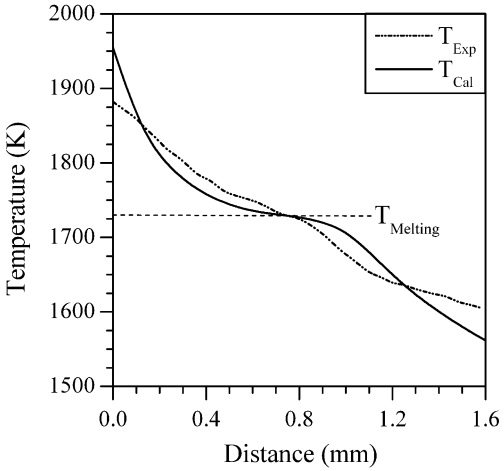


**Fig. 3** Comparison between the computed and the corresponding experimentally measured results [6] along the top surface of the built structure at a point 1.6 mm from the laser beam

Figure 5a–c depicts the influence of laser power ($P$), scanning velocity ($v$), powder mass flow rate ($f$), and idle time ($t_{idle}$) on the computed values of peak temperature and overall thermal cycle at the initial location on the first layer during the deposition of subsequent layers atop it. Figure 5a shows that both the peak temperature and the resident temperature rise with increasing laser power. This is attributed to the increase in net heat input corresponding to greater laser power. Figure 5b depicts that at a constant laser power of 400 W, computed values of peak and the resident temperatures reduce with the increase in scanning velocity and powder mass flow rate. Figure 5c shows that the resident temperature reduces with the increase in the idle time.

**Table 1** Temperature-dependent thermal properties of SS316

| | |
|---|---|
| Density ($\rho$, kg m$^{-3}$) | $8.0 \times 10^3$ |
| Thermal conductivity ($k$, Wm$^{-1}$ K$^{-1}$) | $9.01+0.0152 \times T$ |
| Specific heat ($C$, J kg$^{-1}$ K$^{-1}$) | $363.43+0.407 \times T-0.00018 \times T^2$ |
| Solidus ($T_S$) temperature | 1,693 K |
| Liquidus ($T_L$) temperatures | 1,733 K |
| Latent heat ($L$, J kg$^{-1}$) | $3.0 \times 10^5$ |

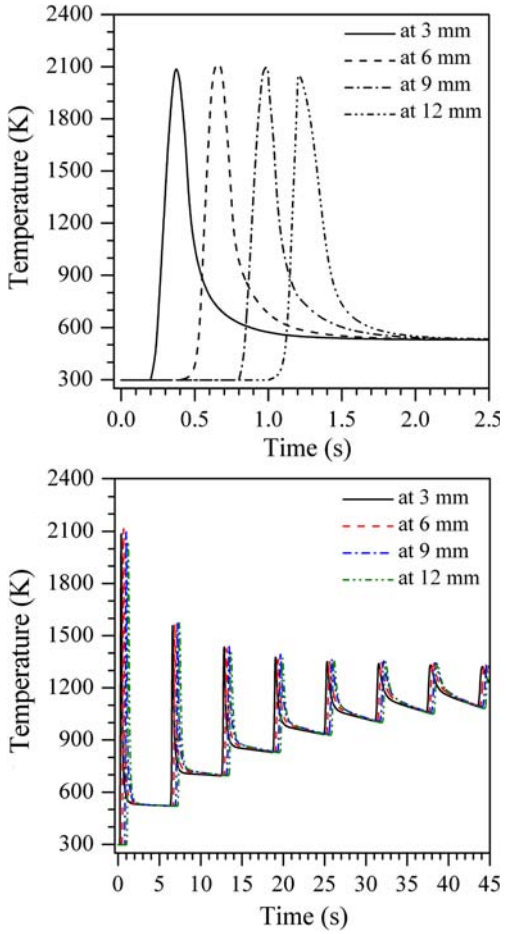


**Fig. 4** Computed thermal cycles experienced at different linear locations (3, 6, 9, and 12 mm from the deposition start point) on the first layer corresponding to a laser power ($P$) of 400 W, scanning velocity ($v$) of 10 mm/s, and powder mass flow rate ($f$) of 4 g/min: **a** during deposition of the first layer; **b** during deposition of first to eighth layers

In LENS™ process, the powder mass flow rate and the scanning velocity must be controlled simultaneously so that the amount of powder injected into the melt pool as well as the rate of powder melting remain uniform throughout the deposition process. Thus, an increase in the scanning velocity is required when the powder mass flow rate is enhanced and vice versa. However, the increase in the scanning velocity at a constant laser power reduces the heat input per unit length resulting in lower peak temperatures and insufficient melting of powder particles, leading to a defective deposition structure. At a constant heat input per unit length, increase or decrease of the powder mass flow rate will lead to the loss of costly powder materials or lack of sufficient powders to create the deposition of a desired width, respectively. Although greater scanning speed assisted with higher laser power is a solution for a faster rate of deposition, vaporization loss of powder material is expected to increase at higher laser powers.

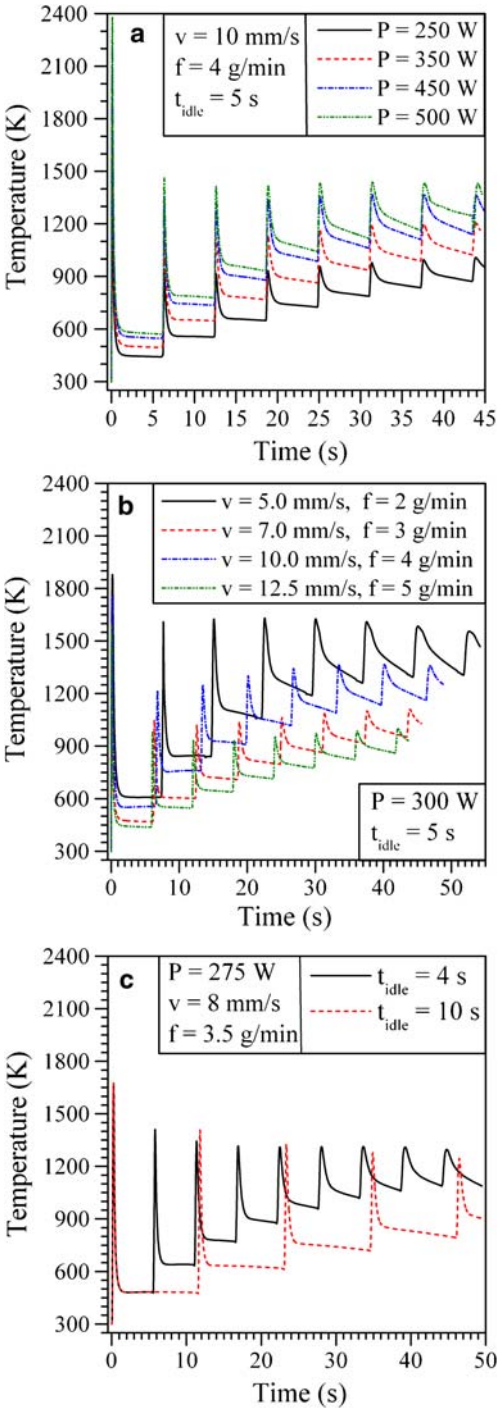


**Fig. 5** Influence of process parameters on computed thermal cycles experienced on the first layer during the deposition of subsequent layers above it: **a** influence of laser power ($P$); **b** influence of scanning velocity ($v$) and powder mass flow rate ($f$); and **c** influence of idle time ($t_{idle}$)

Figure 6a–c shows the computed melt pool dimensions at a build height of 1 mm (~fourth layer) and at a location 7 mm from the left end of the substrate corresponding to a laser power of 400 W and a scanning velocity of 10 mm/s.

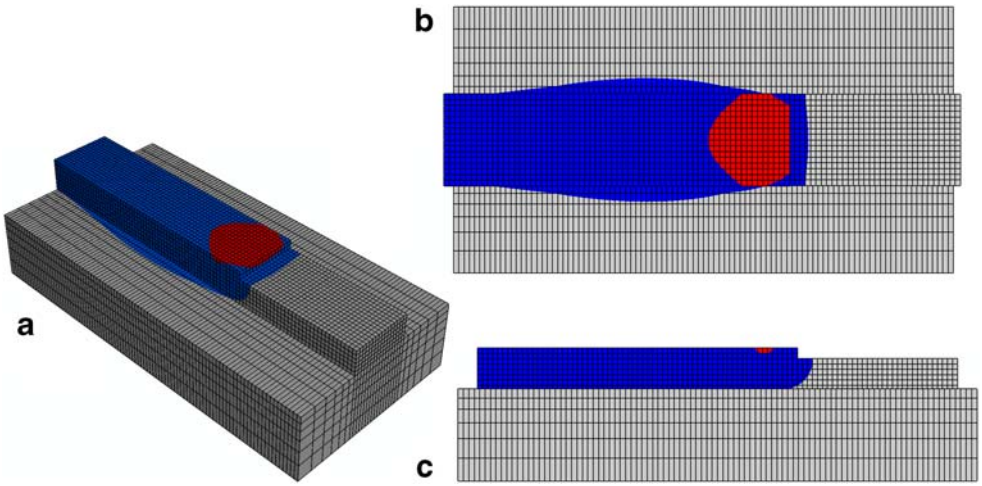


**Fig. 6** Computed melt pool profile along the fourth layer at a location 7 mm from the left end of the substrate: **a** isometric view, **b** top view, **c** front view. Corresponding process parameters are: laser power—400 W, scanning velocity—10 mm/s, and powder mass flow rate—4 g/min

The powder mass flow rate and the catchment efficiency are considered to be 4 g/min and 60%, respectively. The region within the red contour represents temperatures beyond the solidus temperature of SS316 and is conceived to be the melt pool. While Fig. 6a depicts a three-dimensional view of the complete solution domain, Fig. 6b, c show the corresponding top and the front views of the melt pool, respectively, for clarity. Figure 6b depicts that the width of the melt pool is sufficient to form the complete track width, and Fig. 6c shows that the depth of the melt pool is extended up to one layer of bottom elements only. Noting the fact that two layers of elements (height ~0.125 mm) represent one layer of deposition (height ~0.250 mm), it is clear that the current combination of laser power and scanning velocity is insufficient to create a melt pool depth extending up to the previously deposited layer. An improper interlayer bonding is thus expected.

Similar plots are shown in Fig. 7a–c, however, at a higher laser power of 500 W keeping all other parameters constant. Figure 7c clearly shows that the melt pool depth extends through not only the top two layers of elements, which represent the presently depositing layer, but also to the third layer of elements from the top surface that corresponds to part of the previously deposited layer. Figure 7b also shows that the width of the melt pool conforms to the same of layer track continuously. A comparison of Figs. 6 and 7 clearly manifests the need to select the right combination of laser power and scanning velocity for a given powder mass flow rate to ensure proper interlayer material bonding.

Figures 3, 4, 5, 6, and 7 depict that the temperature history and the melt pool dimensions during the deposition process using LENS$^{TM}$ technique depend on several process parameters for a given substrate size and build layer dimensions. The thermophysical material properties of the powder and the substrate materials inherently dictate the choice of the process parameters too. It is often difficult to single out and realize the influence of each parameter on

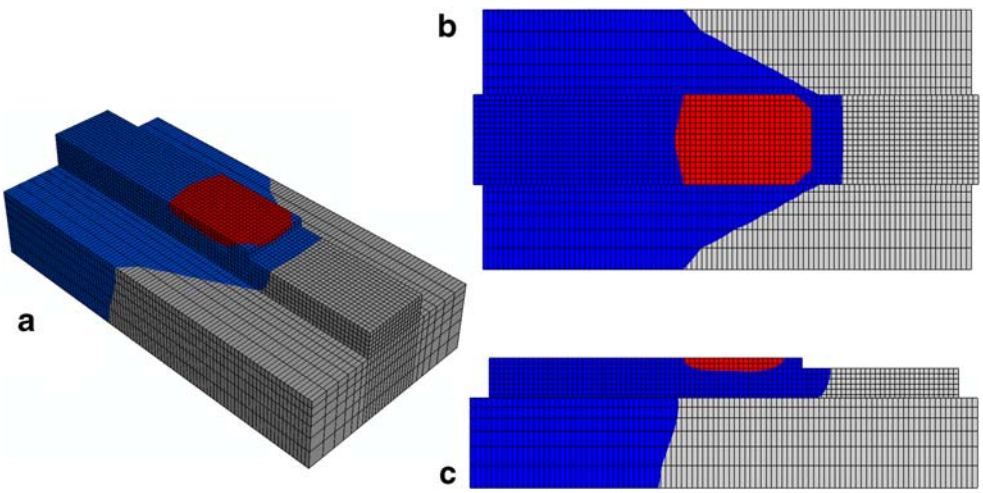


**Fig. 7** Computed melt pool profile along the fourth layer at a location 7 mm from the left end of the substrate: **a** isometric view, **b** top view, **c** front view. Corresponding process parameters are: laser power—500 W, scanning velocity—10 mm/s, and powder mass flow rate—4 g/min

the overall deposition process and, hence, find the optimum combination. A non-dimensional specific energy index, $N_{SP}$, is introduced in the present work, which considers a combined contribution of the significant process parameters in LENS$^{TM}$ technique and the material properties of the powder material. Following a similar number reported in the case of welding, $N_{SP}$ for the LENS$^{TM}$ technique is calculated as [15]:

$$N_{SP} = \frac{\left(\frac{P}{\pi \times r_{lb}^2 \times v}\right)}{[\rho C(T_L - T_a) + \rho L]} \quad (5)$$

where $P$, $r_{lb}$, and $v$ refer to laser power, focused beam radius, and scanning speed, respectively; $\rho$, $C$, $T_L$, $T_a$, and $L$ correspond, respectively, to density, specific heat, liquidus and ambient temperature, and latent heat of melting for the powder materials. In the present work, the values of $\rho$, $C$, $T_L$, $T_a$, and $L$ are considered, respectively, as 8,000 kg/m$^3$, 470 J/kgK, 1693 K, 293 K, and $3.0 \times 10^5$ J/kg. While the numerator in Eq. 5 depicts the incident energy density, the denominator refers to the enthalpy required to heat unit mass of powder material to bring to melting temperature from ambient condition. Furthermore, a minimum and a maximum limit of $N_{SP}$ can be defined as $N_{SP}^{MIN}$ and $N_{SP}^{MAX}$. For a given powder material, it can be conceived that the combination of process parameters leading to values lesser than $N_{SP}^{MIN}$ will be insufficient to create a melt pool dimension required to produce bonding between the layers. Similarly, the combination of process parameters resulting values greater than $N_{SP}^{MAX}$ will lead to the loss of powder particles due to overheating and subsequent vaporization. Values of $N_{SP}^{MIN}$ and $N_{SP}^{MAX}$ can be estimated and documented for a given powder material and also target layer dimensions.

Figure 8a–d shows the variation in $N_{SP}^{MIN}$ and $N_{SP}^{MAX}$ as a function of build height considering powder mass flow rates of 2, 3, 4, and 5 g/min, respectively. The values of $N_{SP}^{MIN}$ and $N_{SP}^{MAX}$, which are obtained through extensive numerical calculations with the developed model, are envisaged to be sufficient to maintain a melt pool depth between 0.3 and 0.5 mm and a minimum melt pool width of 2 mm. To ensure dilution to the immediate layer below and to

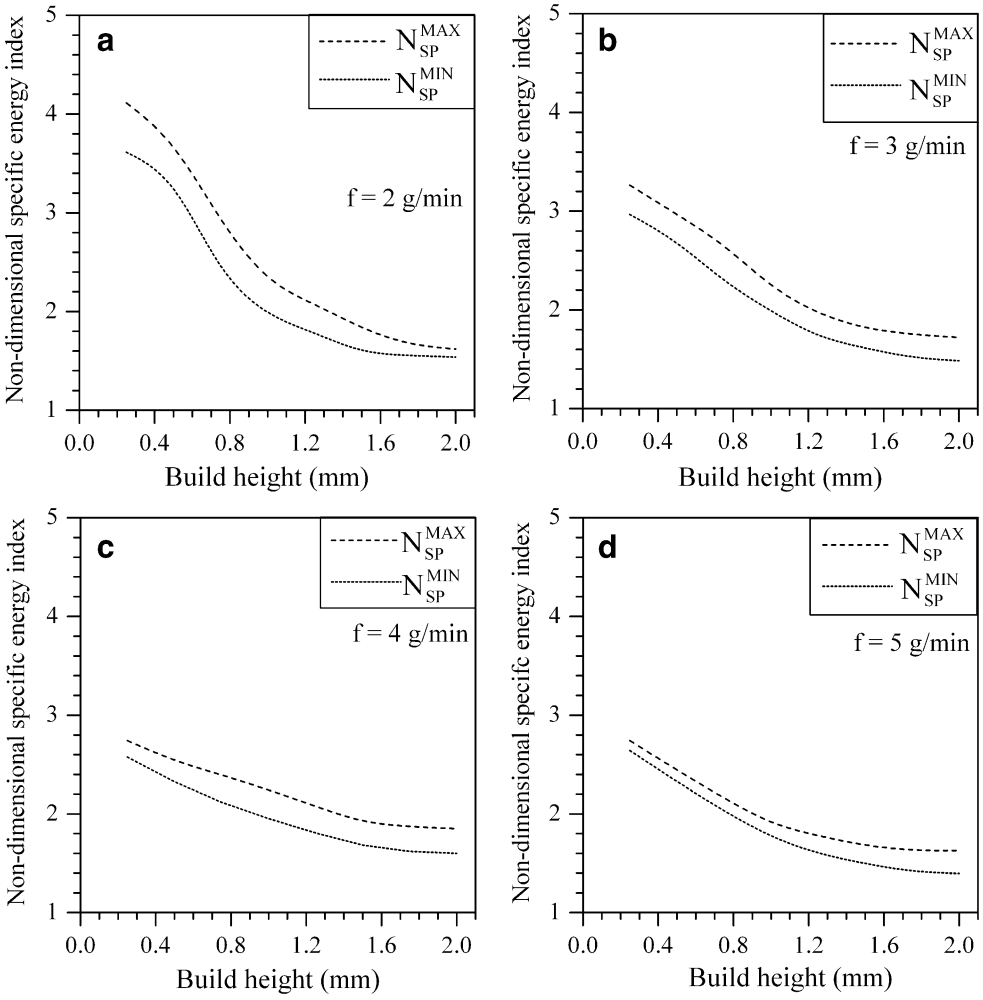


**Fig. 8** Variation in non-dimensional specific energy index as a function of build height for powder mass flow rates of **a** 2 g/min, **b** 3 g/min, **c** 4 g/min, and **d** 5 g/min. $N_{SP}^{MIN}$ and $N_{SP}^{MAX}$ refer, respectively, to the minimum and the maximum values of the non-dimensional parameter

avoid unnecessary deeper penetration when depositing a new layer, a range of 0.3–0.5 mm is set as the target melt pool depth. The target melt pool width corresponds to the desired width of the deposited layer.

Figure 8a–d indicates that the values of $N_{SP}^{MIN}$ and $N_{SP}^{MAX}$ corresponding to a specific powder mass flow rate tend to be insensitive to the build height beyond a certain number of initially deposited layers. The requisite values of both $N_{SP}^{MIN}$and $N_{SP}^{MAX}$ are higher during the deposition of the first two to three layers (i.e., build height ~0.75 mm) and tend to decrease as the build height increases. For the initial few layers, the substrate acts as a heat sink, and hence, greater heat input is required to create and sustain the target melt pool for a given powder mass flow rate. As the build height increases, the influence of the substrate as a heat sink reduces and eventually becomes insignificant. No further variation in process parameters seem to be needed to ensure the target melt pool dimension along any layer deposited above this height.

A comparison of Fig. 8a–d further depicts that the requisite values of both $N_{SP}^{MIN}$ and $N_{SP}^{MAX}$ decrease as the powder mass flow rate increases. This can be attributed to the fact that a greater increase in scanning velocity in comparison to the laser power is associated with higher powder mass flow rate to avoid the loss of the same and maintain the target melt pool dimension. It is, however, noticed that the changes in both $N_{SP}^{MIN}$ and $N_{SP}^{MAX}$ become insignificant beyond a powder mass flow rate of 4 g/min, which possibly is the optimum for the target track dimensions.

The actual values of possible process parameters corresponding to this steady situation is of paramount significance from the design for LENS$^{TM}$ technique point of view. This is depicted in Fig. 9 which outlines five parametric combinations of laser power, scanning velocity, and powder mass flow rate, each of which can yield a steady melt pool width (~track width) and depth of 2 and 0.45 mm, respectively. Each of these combinations is obtained through a number of calculations using the presently developed model. It is thus believed that any of these five sets of process parameters or even any other set along the curve obtained by joining these five combinations in Fig. 9 would result in the steady melt pool dimension as above within an error limit of ±5%. This error limit is conceived from Fig. 3 which manifests a similar range of errors between the computed and the corresponding experimentally measured values of temperature.

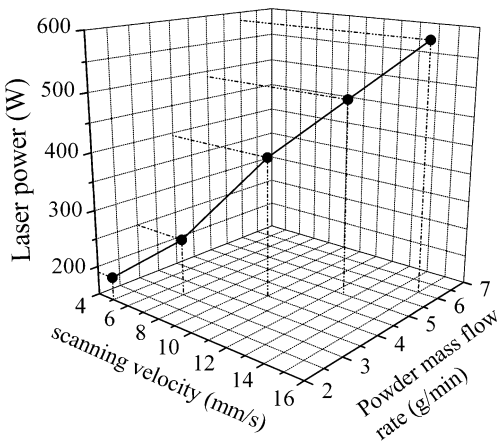


**Fig. 9** Various combinations of laser power, scanning velocity, and powder mass flow rate to achieve a steady melt pool width and penetration of 2 and 0.45 mm, respectively. Melt pool width corresponds to track width

The heat transfer model for LENS$^{TM}$ process developed in this work confirms known experimental trends of temperature profiles. Since LENS$^{TM}$ is a relatively new process with a multitude of possible novel applications, organized research is required to develop quantitative understanding and references for its greater use. The numerical model and the derived results depicted in the present work is a contribution to this direction.

## 4 Conclusion

The present work has reported a three-dimensional heat transfer model to simulate the thermal behavior in LENS$^{TM}$ process using finite element method. The numerical model is developed using the finite element software ABAQUS 6.7 employing the novel element deactivation and activation feature to account for the addition of new elements in the solution domain corresponding to the deposition of powder particles for creating a multilayer structure on a substrate. The influence of critical process parameters on the thermal behavior of each layer during the deposition of subsequent layers above it is analyzed. The model calculations undertake temperature-dependent material properties, latent heat of fusion, and solidification. The following conclusions are arrived at as a part of this present study.

(a) In the LENS$^{TM}$ process, a specific layer undergoes repeated thermal cycles during the deposition of subsequent layers atop it. The peak temperature experienced by a particular layer gradually reduces as the laser beam moves to the higher layers. The melt pool dimensions along a specific layer become steady after the deposition of the initial few layers, except a small portion near the free edges of the deposited layers. The initial few layers are expected to be influenced by the heat loss through the substrate depending on its size.

(b) The deposited layers undergo high cooling rate which is particularly at its highest at the solid–liquid interface and decreasing with the increasing distance from the center of the melt pool.

(c) Laser power, scanning velocity, powder mass flow rate, and idle time between the depositions of successive layers influence the thermal behavior induced in the deposited material. Thus, the final properties and dimensional accuracy of the deposited layers will greatly depend on the synchronization of these parameters.

(d) A non-dimensional specific energy index specific to LENS$^{TM}$ process is introduced which embodies the combined influence of laser power and scanning velocity and the properties of powder materials. It is realized that the laser power and scanning velocity have to be adjusted in a manner as to reduce the value of this non-dimensional number as the build height increases. This conforms to the fact that with the increase in build height, the heat loss towards the substrate is reduced, and thus, heat input per unit length needs to be reduced to avoid over-melting along the top layers. A range of the non-dimensional specific energy index as a function of build height and powder mass flow rate is presented corresponding to typical powder materials and substrate size used in the present modeling work.

## References


1. Griffith M, Keicher D, Atwood C, Romero J, Smugeresky J, Harwell L, Greene D (1996) Freeform fabrication of metallic components using laser engineered net shaping. Solid Freeform Fabrication Proceedings, p 125–132
2. Keicher D, Smugeresky J, Romero J, Griffith M, Harwell L (1997) Using the laser engineered net shaping process to produce complex components from a CAD solid model. Proc SPIE 2993:91–97. doi:10.1117/12.270018
3. Atwood C, Griffith M, Harwell L, Schlienger M, Ensz M, Smugeresky J, Romero J, Greene D, Reckaway D (1998) Laser engineered net shaping (LENS): a tool for direct fabrication of metal parts. Proceedings of the ICALEO, pp E-1–7
4. Griffith M, Schlienger M, Harwell L, Oliver M, Baldwin M, Ensz M, Smugeresky J, Essien M, Brooks J, Robino C, Hofmeister W, Wert M, Nelson D (1999) Understanding thermal behavior in the LENS™ process. J Mater Des 20(2/3):107–113
5. Griffith M, Ensz M, Puskar J, Robino C, Brooks J, Philliber J, Smugeresky J, Hofmeister W (2000) Understanding the microstructure and properties of components fabricated by laser engineered net shaping. Solid Freeform Add Fabr, MRS Symp Proc 625:9–20
6. Hofmeister W, Philliber J, Smugeresky J, Wert M, Ensz M, Griffith M (1999) Investigation of solidification in the laser engineered net shaping process. J Met 7:51–57
7. Vasinonta A, Beuth J, Griffith M (2001) A process map for consistent build conditions in the solid freeform fabrication of thin-walled structures. J Manuf Sci Eng 123(4):615–622. doi:10.1115/1.1370497
8. Costa L, Vilar R, Reti T, Deus A (2005) Rapid tooling by laser powder deposition: process simulation using finite element analysis. Acta Mater 53(14):3987–3999. doi:10.1016/j.actamat.2005.05.003
9. Ye R, Smugeresky J, Zheng B, Zhou Y, Lavernia E (2006) Numerical modeling of the thermal behavior during the LENS process. Mater Sci Eng A 428:47–53. doi:10.1016/j.msea.2006.04.079
10. Wang L, Felicelli S (2006) Analysis of thermal phenomena in LENS deposition. Mater Sci Eng A 435–436:625–631. doi:10.1016/j.msea.2006.07.087
11. Wang L, Felicelli S, Gooroochurn Y, Wang P, Horstemeyer M (2008) Optimization of LENS process for steady molten pool size. Mater Sci Eng A 474(1/2):148–156
12. Grujicic M, Hu Y, Fadel G, Keicher D (2001) Optimization of the LENS rapid fabrication process for in-flight melting of feed powder. J Mater Synth Process 9(5):223–233. doi:10.1023/A:1015262032445
13. Peyre P, Aubry P, Fabbro R, Neveu R, Longuet A (2008) Analytical and numerical modeling of the direct metal deposition laser process. J Phys D Appl Phys 4:1–10
14. ABAQUS ref. manual (2001) Chp. 6—heat transfer analysis. Hibbitt, Karlson & Sorensen, Pawtucket, RI
15. De A, DebRoy T (2004) A smart model to determine effective thermal conductivity and viscosity in the weld pool. J Appl Phys 95:5230–5240. doi:10.1063/1.1695593